Journal of Molecular Structure xxx (2014) xxx–xxx

Contents lists available at ScienceDirect

Journal of Molecular Structure

journal homepage: www.elsevier.com/locate/molstruc

Study of supramolecular frameworks having aliphatic dicarboxylic acids, *N*,*N*′-bis(salicyl)ethylenediamine and *N*,*N*′-bis(salicyl)butylenediamine

Nidhi Goel [a,*], Naresh Kumar [b]

[a] Department of Chemistry, Indian Institute of Technology Roorkee, Roorkee 247 667, India
[b] Department of Biotechnology, Indian Institute of Technology Roorkee, Roorkee 247 667, India

HIGHLIGHTS

- Six new salts of dicarboxylic acids with *N*,*N*′-bis(salicyl)alkylenediamines.
- Detailed X-ray crystallographic study for salts.
- Comparison of solid and gaseous phase structure for salts.
- Curve fitting analysis between experimental and theoretical values.

GRAPHICAL ABSTRACT

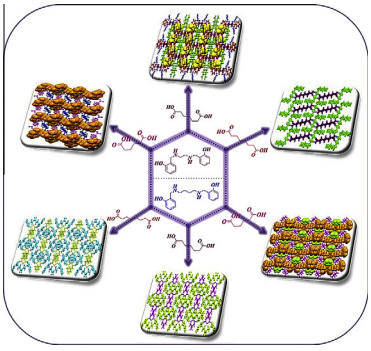

ARTICLE INFO

Article history:
Received 23 January 2014
Received in revised form 19 April 2014
Accepted 19 April 2014
Available online xxxx

Keywords:
N,*N*′-bis(salicyl)ethylenediamine
N,*N*′-bis(salicyl)butylenediamine
Dicarboxylic acids
Hydrogen bond interactions
Density functional theory
Supramolecular framework

ABSTRACT

The reaction of bases (L_1 and L_2) (where L_1 = *N*,*N*′-bis(salicyl)ethylenediamine, L_2 = *N*,*N*′-bis(salicyl)butylenediamine) with dicarboxylic acids [adipic acid (1,6-Hexanedioic acid, AA), pimelic acid (1,7-Heptanedioic acid, PA) and suberic acid (1,8-Octanedioic acid, SUA] yielded the corresponding six new ionic salts viz., $[1/2L_1H^+\cdot 1/2AA^-\cdot 1/2AA]$ (**1**), $[2\times 1/2L_1H^+\cdot PA^{2-}\cdot CHCl_3]$ (**2**) $[1/2L_1H^+\cdot 1/2SUA^-]$ (**3**), $[1/2L_2H^+\cdot 1/2AA^-\cdot 2CH_3OH]$ (**4**), $[1/2L_2H^+\cdot 1/2PA^-]$ (**5**) and $[1/2L_2H^+\cdot 1/2SUA^-]$ (**6**), respectively. Theses salts were characterized by elemental analysis, FT-IR, NMR, X-ray crystallography, and theoretically by means of Gaussian 09. The X-ray crystallographic studies revealed that the proton transfer occurred from acid to base. It also demonstrated that different type of hydrogen bond interactions between cations and anions were responsible for the supramolecular frameworks. The optimized structures of these salts were calculated in terms of the density functional theory. The curve fitting analysis between experimental and simulated data of structural parameters was done, and found statistically close. The orientation of molecules was remained same in both the gas and solid phases. The thermal studies of these salts were investigated by TG–DTG.

Introduction

Supramolecular chemistry is an expanding area of research for the creation of new cocrystals, ionic salts and molecular complexes, which exhibits the structural novelty and diversity [1–6]. Noncovalent interactions are responsible for the designing of supramolecular frameworks, where the molecules interact with each other, and form a highly ordered crystalline materials [7–13]. Among the various noncovalent interactions, hydrogen bond is the most important, and intensively studied in the structural chemistry as well as in biology due to its strength, high degree of directionality, and participation in construction of robust supramolecular synthons [14–19]. In this context, Etter gave a guideline

* Corresponding author. Tel.: +91 09412841504.
E-mail address: nidhigoel.iitr@gmail.com (N. Goel).

http://dx.doi.org/10.1016/j.molstruc.2014.04.064
0022-2860/

regarding the hydrogen-bond interactions, "the best donor in the molecule preferentially interacts with the best acceptor in the system, the second best donor–acceptor group hydrogen bond next, and so on" [20]. The carboxylic acids are the most popular functional groups, and play a significant role in forming the directional and robust synthons [21,22]. It is well known that the carboxylic acids have both hydrogen bond donor and acceptor groups that are self-associated through O—H···O hydrogen bonds, and are involved in the formation of supramolecular homosynthons, while on the other side the same functional group has been extensively used as a strong hydrogen bond donor to a variety of nitrogen containing hydrogen bond acceptors, and is resulted in the formation of supramolecular heterosynthons. Due to these attractive features, carboxylic acids have been used for cocrystallization by several workers [23–31], but their use in cocrystallization with *N*,*N*′-bis(salicyl)ethylenediamine (L_1) and *N*,*N*′-bis(salicyl)butylenediamine (L_2) as one component are not yet reported. These bases are important organic compounds, and may be used for assembling the diverse architectures in the area of supramolecular chemistry as molecular building blocks control the molecular packing in crystalline materials due to presence of donor and acceptor functional groups. The purpose of this work is to cocrystallize the selected dicarboxylic acids with bases (L_1 and L_2), and also see the effect of increasing carbon chain in acids and bases on the supramolecular frameworks and hydrogen bond interaction energy of these salts. This paper reports the syntheses, crystal structures, theoretical, thermal studies of newly constructed ionic salts, and also presents the significant role of these bases in the formation of well-designed and long-range structures.

Experimental section

Materials

All manipulations were performed in air using commercial grade solvents. *N*,*N*′-bis(salicyl)ethylenediamine (L_1) and *N*,*N*′-bis(salicylidene)butylenediamine were prepared by the known procedure [32,33]. Adipic acid (1,6-Hexanedioic acid, AA), pimelic acid (1,7-Heptanedioic acid, PA) and suberic acid (1,8-Octanedioic acid, SUA) were purchased from Aldrich Chemical Company, USA.

Synthesis of N,N′-bis(salicyl)butylenediamine and salts

The salts **1–6**, were synthesized by the stoichiometric combination of L_1, L_2 and dicarboxylic acids (AA/PA/SUA) as shown in Schemes 1 and 2.

Synthesis of N,N′-bis(salicyl)butylenediamine (L_2)

N,*N*′-bis(salicylidene)butylenediamine (5.93 g, 20.0 mmol) was dissolved in 50.0 ml of methanol. Then to this solution, sodium borohydride (1.52 g, 40.0 mmol) was added slowly at 45 °C. The reaction mixture was refluxed for 6 h at 60 °C. The precipitate obtained by addition of water, was filtered, and recrystallized from methanol at 4 °C in 79.3% (0.24 g, 0.79 mmol) yield. Anal. Calcd. (%) for $C_{18}H_{24}N_2O_2$ (300.18): C, 71.97; H, 8.04; N, 9.33; Found: C, 71.67; H, 7.94; N, 9.11. FT-IR (KBr, cm^{-1}): 3519, 3439, 3033, 2937, 2815, 2083, 1899, 1779, 1651, 1602, 1449, 1273, 1169, 939, 753, 617, 504. ^{1}H NMR (DMSO-d_6, ppm) δ: 2.59 (s, 4H, CH_2, Benzylic), 3.40 (m, 4H, CH_2, aliphatic), 3.90 (m, 4H, CH_2, aliphatic), 6.71–6.77 (m, 4H, CH, Ar), 7.06–7.14 (m, 4H, CH, Ar), 12.04 (s, br, 2H, NH).

*Synthesis of salt **1***

Salt **1** was prepared by mixing L_1 (0.27 g, 1.0 mmol) and AA (0.15 g, 1.0 mmol) in an acetonitrile-methanol mixture (v/v%, 1:4, 10 ml). The resulting solution was stirred for 6 h, and filtered through Celite. The filtrate was evaporated until dryness under vacuum, and the white solid obtained was redissolved in methanol. The colorless crystals of **1** in 72.5% (0.41 g, 0.72 mmol) yields, suitable for X-ray data collection were obtained by slow evaporation of solvent at room temperature. Anal. Calcd. (%) for $C_{28}H_{40}N_2O_{10}$ (564.62): C, 59.56; H, 7.13; N, 4.96. Found: C, 59.12; H, 7.01; N, 4.73. FT-IR (KBr, cm^{-1}): 3669, 3332, 3077, 2951, 2869, 2671, 2292, 1686, 1426, 1365, 1272, 1127, 1029, 926, 739, 677, 519. ^{1}H NMR (DMSO-d_6, ppm) δ: 12.14 (s, br, 4H, NH_2), 6.10–6.74 (m, 8H, CH, Ar L_1), 3.21 (t, 4H, CH_2, aliphatic L_1), 2.34 (s, 4H, CH_2, Benzylic L_1), 2.12 (m, 4H, CH_2, AA^{2-}), 1.37 (t, 4H, CH_2, AA^{2-}).

*Synthesis of salt **2***

Salt **2** was obtained by the same procedure as outlined above for **1** using PA (0.16 g, 1.0 mmol) in chloroform–methanol mixture (v/v%, 1:4, 10 ml) with 69.8% (0.68 g, 0.69 mmol) yields. Anal. Calcd. (%) for $C_{47}H_{65}N_4O_{12}Cl_3$ (984.40): C, 57.34; H, 6.65; N, 5.69; Found: C, 57.07; H, 6.55; N, 5.49. FT-IR (KBr, cm^{-1}): 3643, 3324, 2949, 2411, 2269, 2161, 1933, 1697, 1567, 1412, 1354, 1139, 1033, 922, 739, 697, 526. ^{1}H NMR (DMSO-d_6, ppm) δ: 12.37 (s, br, 4H, NH_2), 6.07–6.62 (m, 8H, CH, Ar L_1), 3.19 (t, 4H, CH_2, aliphatic L_1), 2.31 (s, 4H, CH_2, Benzylic L_1), 2.17 (t, 4H, CH_2, PA^{2-}), 1.55 (m, 4H, CH_2, PA^{2-}), 1.29 (m, 2H, CH_2, PA^{2-}).

*Synthesis of salt **3***

The same procedure was applied on salt **3** as outlined above for **1** using SUA (0.17 g, 1.0 mmol) with 77.7% (0.35 g, 0.78 mmol) yields. Anal. Calcd. (%) for $C_{24}H_{34}N_2O_6$ (446.54): C, 64.55; H, 7.67; N, 6.27. Found: C, 63.87; H, 7.56; N, 6.53. FT-IR (KBr, cm^{-1}): 3659, 3337, 2945, 2845, 2759, 2617, 2259, 2049, 1611, 1529, 1455, 1377, 1256, 1109, 1057, 931, 841, 791, 529. ^{1}H NMR (DMSO-d_6, ppm) δ: 12.21 (s, br, 4H, NH_2), 5.99–6.59 (m, 8H, CH, Ar L_1), 3.18 (t, 4H, CH_2, aliphatic L_1), 2.29 (s, 4H, CH_2, Benzylic

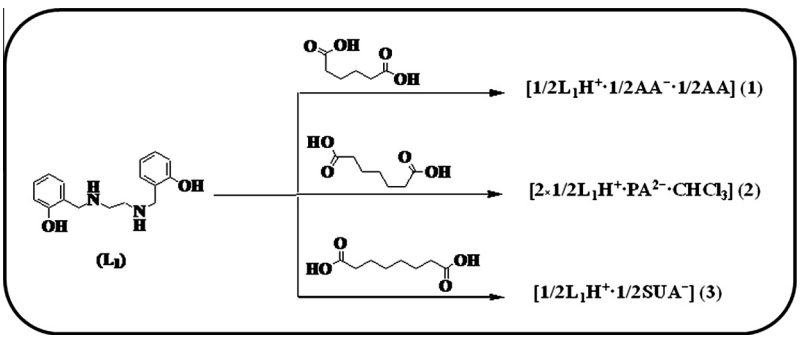

Scheme 1. General method for preparation of salts **1–3**.

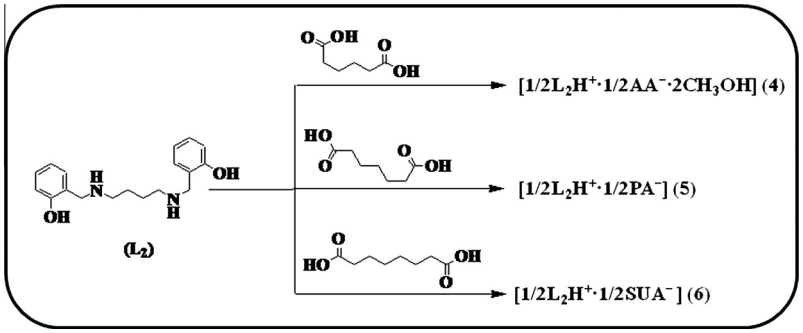

Scheme 2. General method for preparation of salts **4–6**.

L_1), 2.16 (t, 4H, CH_2, SUA^{2-}), 1.54 (t, 4H, CH_2, SUA^{2-}), 1.28 (m, 4H, CH_2, SUA^{2-}).

*Synthesis of salt **4***

Salt **4** was obtained by the same procedure as outlined above for **1** using L_2 (0.30 g, 1.0 mmol) and AA (0.15 g, 1.0 mmol) with 77.8% (0.40 g, 0.78 mmol) yields. Anal. Calcd. (%) for $C_{26}H_{42}N_2O_8$ (510.62): C, 61.15; H, 8.28; N, 5.48; Found: C, 60.91; H, 8.23; N, 5.36. FT-IR (KBr, cm^{-1}): 3545, 3326, 2957, 2663, 2561, 1623, 1541, 1419, 1279, 1112, 1039, 927, 749, 611. ^{1}H NMR (DMSO-d_6, ppm) δ: 12.33 (s, br, 4H, NH_2), 7.03–7.11 (m, 4H, CH, Ar L_2), 6.69–6.74 (m, 4H, CH, Ar L_2), 3.84 (m, 4H, CH_2, aliphatic L_2), 3.37 (m, 4H, CH_2, aliphatic L_2), 2.54 (s, 4H, CH_2, Benzylic L_2), 2.13 (m, 4H, CH_2, AA^{2-}), 1.41 (t, 4H, CH_2, AA^{2-}).

*Synthesis of salt **5***

Salt **5** was obtained by the same procedure as outlined above for **4** using PA (0.16 g, 1.0 mmol) with 69.3% (0.32 g, 0.69 mmol) yields. Anal. Calcd. (%) for $C_{25}H_{36}N_2O_6$ (460.56): C, 65.19; H, 7.87; N, 6.08. Found: C, 64.92; H, 7.69; N, 5.89. FT-IR (KBr, cm^{-1}): 3589, 3330, 2940, 2869, 2700, 2556, 1621, 1504, 1408, 1123, 1065, 922, 790, 673. ^{1}H NMR (DMSO-d_6, ppm) δ: 12.19 (s, br, 4H, NH_2), 7.04–7.09 (m, 4H, CH, Ar L_2), 6.64–6.71 (m, 4H, CH, Ar L_2), 3.81 (m, 4H, CH_2, aliphatic L_2), 3.33 (m, 4H, CH_2, aliphatic L_2), 2.51 (s, 4H, CH_2, Benzylic L_2), 2.18 (t, 4H, CH_2, PA^{2-}), 1.61 (m, 4H, CH_2, PA^{2-}), 1.33 (m, 2H, CH_2, PA^{2-}).

*Synthesis of salt **6***

Salt **6** was obtained by the same procedure as outlined above for **4** using SUA (0.17 g, 1.0 mmol) with 72.9% (0.35 g, 0.73 mmol) yields. Anal. Calcd. (%) for $C_{26}H_{38}N_2O_6$ (474.58): C, 65.80; H, 8.06; N, 5.90. Found: C, 65.33; H, 7.95; N, 5.69. FT-IR (KBr, cm^{-1}): 3788, 3320, 3032, 2941, 2863, 2604, 2543, 2360, 1610, 1541, 1430, 1253, 1121, 1004, 795, 682. ^{1}H NMR (DMSO-d_6, ppm) δ: 12.23 (s, br, 4H, NH_2), 7.02–7.07 (m, 4H, CH, Ar L_2), 6.66–6.73 (m, 4H, CH, Ar L_2), 3.84 (m, 4H, CH_2, aliphatic L_2), 3.35 (m, 4H, CH_2, aliphatic L_2), 2.53 (s, 4H, CH_2, Benzylic L_2), 2.18 (t, 4H, CH_2, SUA^{2-}), 1.57 (t, 4H, CH_2, SUA^{2-}), 1.31 (m, 4H, CH_2, SUA^{2-}).

Instrumentation

Crystallized salts were carefully dried under vacuum for several hours prior to elemental analysis on Elementar Vario EL III analyzer. FT-IR spectra were obtained on a Thermo Nikolet Nexus FT-IR spectrometer in KBr pellets. ^{1}H NMR spectra were recorded on Bruker-D-Avance 500 MHz spectrometer with Fourier transform technique using TMS as internal standard. Thermogravimetry

Table 1
Crystallographic data and structure refinement parameters for salts **1–6**.

	Salt **1**	Salt **2**	Salt **3**	Salt **4**	Salt **5**	Salt **6**
Empirical formula	$C_{28}H_{40}N_2O_{10}$	$C_{24}H_{33}N_2O_6Cl_3$	$C_{24}H_{34}N_2O_6$	$C_{26}H_{42}N_2O_8$	$C_{25}H_{36}N_2O_6$	$C_{26}H_{38}N_2O_6$
Formula weight	564.62	551.87	446.53	510.62	460.56	474.58
Temprature	296(2)	296(2)	296(2)	296(2)	296(2)	296(2)
Crystal system	Triclinic	Monoclinic	Triclinic	Monoclinic	Monoclinic	Monoclinic
Space group	*P*–1	*C* 2/*c*	*P*–1	*P*21/*c*	*C* 2/*c*	*C* 2/*c*
a (Å)	8.528(5)	22.825(4)	5.824(3)	8.547(14)	18.518(6)	18.455(17)
b (Å)	8.914(5)	13.896(4)	7.679(5)	22.146(4)	9.396(3)	9.179(7)
c (Å)	9.704(6)	19.379(5)	13.744(8)	7.355(13)	13.959(5)	15.271(12)
α (°)	73.91(3)	90.00	97.26(3)	90.00	90.00	90.00
β (°)	88.95(3)	114.92(17)	98.18(3)	100.00(9)	91.81(2)	95.28(7)
γ (°)	79.12(3)	90.00	101.16(3)	90.00	90.00	90.00
V (Å^3)	695.67(7)	5574(2)	589.3(6)	1371.2(4)	2427.5(13)	2576.3(4)
Z	1	8	1	2	4	4
D_{calc} (g/cm^3)	1.348	1.315	1.258	1.237	1.260	1.224
μ(Mo Kα) (cm^{-1})	0.102	0.368	0.090	0.091	0.090	0.086
F(000)	302	2320.0	240.0	552	992	1024
Crystal size	0.3 × 0.24 × 0.19	0.27 × 0.21 × 0.16	0.21 × 0.18 × 0.14	0.29 × 0.23 × 0.17	0.31 × 0.27 × 0.21	0.26 × 0.19 × 0.13
Theta range for data collection (°)	2.19–30.68	1.77–28.37	2.74–28.59	2.96–28.36	2.20–28.36	2.68–28.43
No. of measured reflections	4249	6893	2744	3329	2984	3179
No. of observed reflections	3548	4650	1406	2365	1663	1559
Data/restraints/parameters	4249/0/186	6893/0/318	2744/0/146	3329/0/166	2984/0/151	3179/0/155
Goodness-of-fit	0.920	2.097	0.828	1.400	1.060	1.141
Final *R* indices[$I > 2(I)$ R_1[a]	0.0383	0.0971	0.0715	0.0738	0.0768	0.0813
wR_2[b]	0.1177	0.1953	0.1647	0.2172	0.1925	0.1943

[a] $R_1 = \sum||F_o|-|F_c||/\sum|F_o|$.
[b] $wR_2 = \{\sum [w (F_o^2-F_c^2)^2]/\sum w (F_o^2)^2$.

and derivative thermogravimetry (TG–DTG) were carried out at 10 °C/min (mass 0.055 g) under a nitrogen atmosphere (flow rate of 200 ml/min) on PerkinElmer's (Pyris Diamond) (Woodland, California, USA) thermogravimetric analyzer.

X-ray diffraction data

Single crystal X-ray diffraction data were collected at 100 K on a Bruker Kappa four circle-CCD diffractometer using graphite monochromated Mo Kα radiation (λ = 0.71070 Å). Empirical absorption corrections were applied in the reduction of data Lorentz and polarization corrections [34]. The SHELXTL program was used for the structure solution, refinement and data output [35,36]. Non-hydrogen atoms were refined anisotropically, while the hydrogen atoms were placed in geometrically calculated positions by using a riding model. Images and hydrogen bonding interactions were created with DIAMOND and MERCURY softwares [37,38]. The crystallographic data and the selected hydrogen bond distances are given in Tables 1 and 2, respectively.

Computational and statistical analysis

Geometry optimization of the different ionic salts was done by Gaussian 09 program at B3LYP/6-311G^{++}(d,p) basis set [39–41]. The input for the simulation was Z-matrix generalized by Gaussview 5.0 that was also used for visualizing the molecules with optimized geometries. ChemCraft, version 1.5 software was used for comparing the optimized structure with the crystallographic one. The experimental and simulated values for bond lengths and bond angles were statistically tested for significance in MATLAB R2010a toolbox that is used for measuring the potency and direction of a linear association between two variables.

Results and discussions

Infrared and NMR spectroscopy

As compared to free carboxylic acids (1673 and 1737 cm^{-1}), the C=O stretching bands appear in the range 1592 and 1650 cm^{-1} for salts **1–6**. The NH stretching vibration is normally observed at 3500–3400 cm^{-1}, which is shifted to lower wavenumber (Tables S1 and S2). The shifting towards lower frequency is due to the hydrogen bonded noncovalent interactions between —NH protons donor and carboxylate anion acceptor [42–44]. The presence of hydrogen bond interactions in the solution for **1–6** was confirmed by the prominent downfield chemical shift in the ^{1}H NMR spectra of each case with respect to the free ligand.

*Structure description of salts **1–6***

Salt **1** is crystallized in the triclinic system with space group *P*−1. An asymmetric unit consists of half molecule of protonated base ($L_1H_2^{2+}$), half molecule of deprotonated adipate ion (AA^{2-}) and half molecule of neutral adipic acid (AA). In **1**, the acidic hydrogen of the carboxyl group on adipic acid was transferred to the nitrogen atom of base as shown in Fig. 1. The protonated nitrogen (N1) shows the strong hydrogen bonding with the oxygen atoms (O3, O4) of adipic acid and adipate anion via N—H···O [N1—H1A···O3, 1.921 (9) Å; N1—H1B···O4, 1.848(7) Å] intermolecular interactions. The crystal packing also shows other O—H···O [O1—H1···O5, 1.894(9) Å; O2—H2A···O4, 1.608(27) Å], C—H···O [C10—H10A···O2, 2.814(10) Å] and C—H···π [C7—H7B···π, 3.474(53) Å] noncovalent interactions (Fig. S1). All hydrogen bonded interactions are in good agreement with the reported values [45,28]. These interactions are involved in the formation of a cavity through protonated bases and adipate anions for the accommodation of neutral adipic acid, where adipic acid acts as a guest molecule. The presence of different noncovalent interactions is resulted in the creation of three dimensional host–guest supramolecular framework along '*a*' axis (Fig. 2).

The salt **2** with two half molecules of protonated base ($L_1H_2^{2+}$), one molecule of pimelate ion (PA^{2-}) and one molecule of chloroform in asymmetric unit crystallizes in monoclinic system with space group *C* 2/*c* as shown in Fig. 3. The protonated nitrogen atoms (N1, N2) of bases present the strong hydrogen bonding with the oxygen atoms (O3, O4, O5, O6) of pimelate ion via N—H···O [N1—H1B···O6, 1.881(29) Å; N1—H1C···O3, 1.846(28) Å; N2—H2B···O5, 2.759(30) Å; N2—H2B···O6, 1.906(25) Å;

Table 2
Noncovalent interactions for salts **1–6** (Å and °).

D—H···A	d(D—H)	d(H—A)	d(D—A)	⟨(DHA)⟩
*Salt **1***				
N1—H1A···O3	0.900	1.921 (9)	2.820(13)	177.3
N1—H1B···O4	0.900	1.848(7)	2.659(11)	156.0
O1—H1···O5	0.820	1.894(9)	2.696(13)	165.6
O2—H2A···O4	0.970	1.608(27)	2.533(12)	175.9
C10—H10A···O2	0.970	2.814(10)	3.620(16)	141.0
C7—H7B···π	0.970	3.474(53)	3.808(10)	102.7
*Salt **2***				
N1—H1B···O6	0.900	1.881(29)	2.743(42)	159.8
N1—H1C···O3	0.900	1.846(28)	2.675(38)	152.2
N2—H2B···O5	0.900	2.759(30)	3.492(37)	139.4
N2—H2B···O6	0.900	1.906(25)	2.789(35)	166.3
N2—H2C···O4	0.900	2.412(46)	3.049(49)	127.9
O1—H1···O5	0.821	1.759(38)	2.561(51)	164.8
O2—H2A···O4	0.821	2.310(92)	3.021(91)	145.1
C2—H2···O5	0.929	2.650(38)	3.280(61)	125.6
C8—H8A···O3	0.970	2.643(27)	3.316(44)	126.8
C8—H8B···O6	0.970	2.569(24)	3.287(42)	130.8
C13—H13···O5	0.930	2.528(29)	3.387(46)	153.7
C15—H15···O4	0.970	2.883(89)	3.389(74)	123.5
C16—H16B···O4	0.970	2.864(70)	3.331(61)	121.8
*Salt **3***				
N1—H1A···O2	0.899	1.831(23)	2.677(34)	155.6
N1—H1A···O3	0.899	2.548(34)	3.336(42)	146.6
N1—H1B···O3	0.900	1.796(33)	2.693(42)	174.3
O1—H1···O2	0.819	1.808(27)	2.573(38)	154.6
C5—H5···O3	0.930	2.601(32)	3.269(47)	129.2
C8—H8A···O3	0.970	2.818(31)	3.489(43)	127.0
C8—H8B···O2	0.969	2.933(27)	3.559(38)	123.3
C8—H8B···O3	0.969	2.908(37)	3.631(48)	132.2
C10—H10A···π	0.969	3.259(16)	4.123(38)	149.4
*Salt **4***				
N1—H1A···O2	0.900	1.810(8)	2.709	176.8
N1—H1A···O3	0.900	2.816(5)	3.461	129.7
N1—H1B···O2	0.900	2.087(2)	2.860	143.2
O4—H4···O1	0.820	2.888(9)	3.395	121.9
C4—H4A···O4	0.931	3.162(9)	3.833	130.5
C5—H5···O3	0.930	3.469(9)	4.148	131.8
C5—H5···O4	0.930	3.401(18)	3.957	120.6
C7—H7A···O3	0.970	2.933(6)	3.592	126.2
C9—H9A···O2	0.970	2.532(9)	3.317	138.0
C9—H9B···O2	0.970	3.116(8)	3.657	116.8
C13—H13B···O1	0.960	3.082(6)	3.526	109.9
*Salt **5***				
N1—H1A···O2	0.900	1.949(4)	2.715	142.0
N1—H1B···O3	0.900	1.898(2)	2.765	161.0
O1—H1···O3	0.820	1.815(6)	2.631	173.2
C8—H8B···π	0.970	3.250(3)	4.217	174.9
*Salt **6***				
N1—H1A···O3	0.899	2.748(4)	3.112	125.5
N1—H1B···O2	0.900	1.872(2)	2.759	168.2
N1—H1B···O3	0.900	2.643(7)	3.112	132.3
O1—H1···O1	0.819	2.855(3)	3.261	112.8
O1—H1···O2	0.819	1.860(3)	2.653	162.8
C2—H2···O2	0.970	2.765(6)	3.396	125.8
C9—H9A···O2	0.970	2.923(10)	3.591	126.9
C11—H11A···O1	0.970	2.647(8)	3.235	123.3
C8—H8A···π	0.970	3.541(10)	4.477	162.7

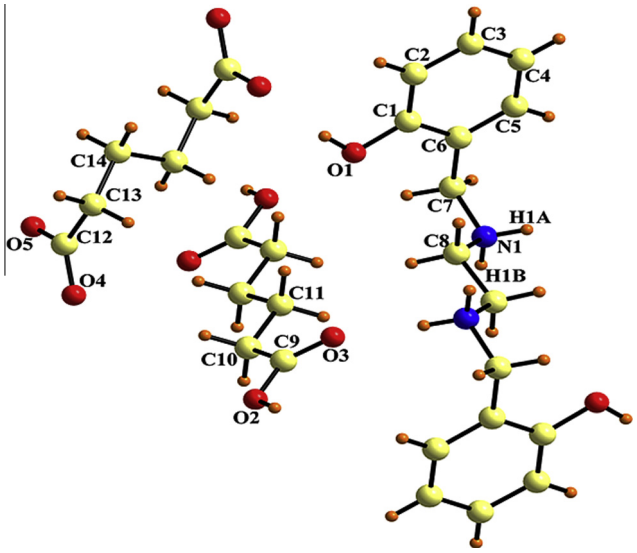

Fig. 1. Molecular structure of salt **1**. Color code: C, yellow; H, orange; O, red; N, blue. (For interpretation of the references to colour in this figure legend, the reader is referred to the web version of this article.)

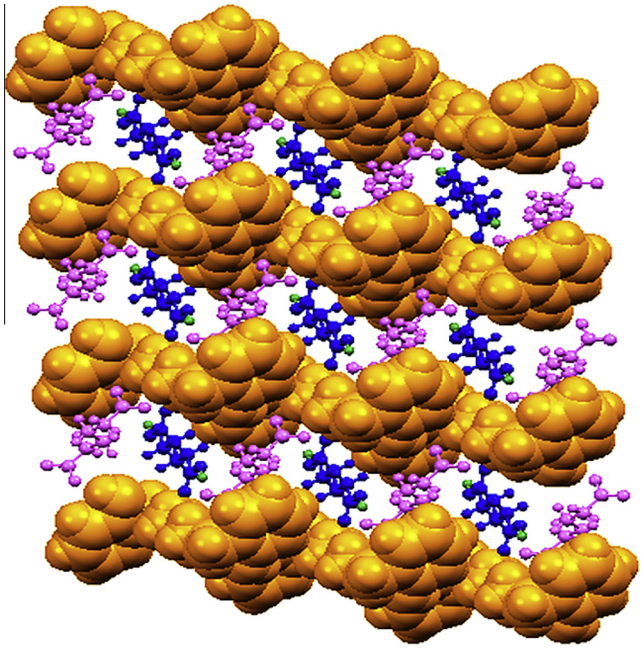

Fig. 2. Three dimensional host–guest supramolecular framework in **1**. Color code: protonated base, orange; adipate ion, pink; adipic acid, blue. (For interpretation of the references to colour in this figure legend, the reader is referred to the web version of this article.)

N2—H2C···O4, 2.412(46) Å] intermolecular interactions. Other noncovalent interactions such as O—H···O [O1—H1···O5, 1.759(38) Å; O2—H2A···O4, 2.310(92) Å] and C—H···O [C2—H2···O5, 2.650(38) Å; C8—H8A···O3, 2.643(27) Å; C8—H8B···O6, 2.569(24) Å; C13—H13···O5, 2.528(29) Å; C15—H15···O4, 2.883(89) Å; C16—H16B···O4, 2.864(70) Å] are also present (Fig. S2a). According to Fig. S2b, the chloroform molecule is bonded with the pimelate ion through very weak Cl2···O4, 3.043(23) Å noncovalent interaction [46,47]. Due to the presence of various noncovalent interactions, these acids and bases with solvent molecules provide the mat like perspective view along the '*c*' axis (Fig. 4).

The cocrystallization of base (L_1) with suberic acid give salt **3**. It crystallizes in triclinic system with space group *P*−1, and contains half molecule of protonated base ($L_1H_2^{2+}$) and half molecule of suberate anion (Fig. 5). As shown in Fig. S3, one molecule of cationic base holds the three molecules of suberate anions through the different N—H···O [N1—H1A···O2, 1.831(23) Å; N1—H1A···O3, 2.548(34) Å; N1—H1B···O3, 1.796(33) Å], O—H···O [O1—H1···O1, 1.808(27) Å], C—H···O [C5—H5···O3, 2.601(32) Å; C8—H8A···O3, 2.818(31) Å; C8—H8B···O2, 2.933(27) Å; C8—H8B···O3, 2.908(37) Å] and C—H···π [C10—H10A···π, 3.259(16) Å] noncovalent interactions [48]. Various hydrogen bonded interactions between protonated bases and suberate anions give the three dimensional ladder like packing view along the '*a*' axis with three different types of peudocavities (Fig. 6).

Salt **4** is crystallized in the monoclinic system with space group *P*21/*c*. An asymmetric unit consists of half molecule of protonated base ($L_2H_2^{2+}$), half molecule of deprotonated adipate ion (AA^{2-}) and

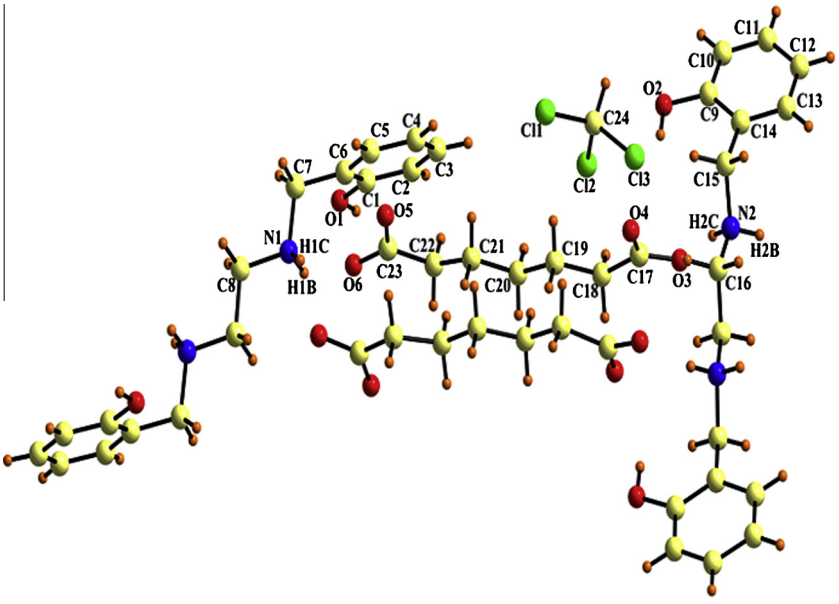

Fig. 3. Molecular structure of salt **2**. Color code: C, yellow; H, orange; O, red; N, blue. (For interpretation of the references to colour in this figure legend, the reader is referred to the web version of this article.)

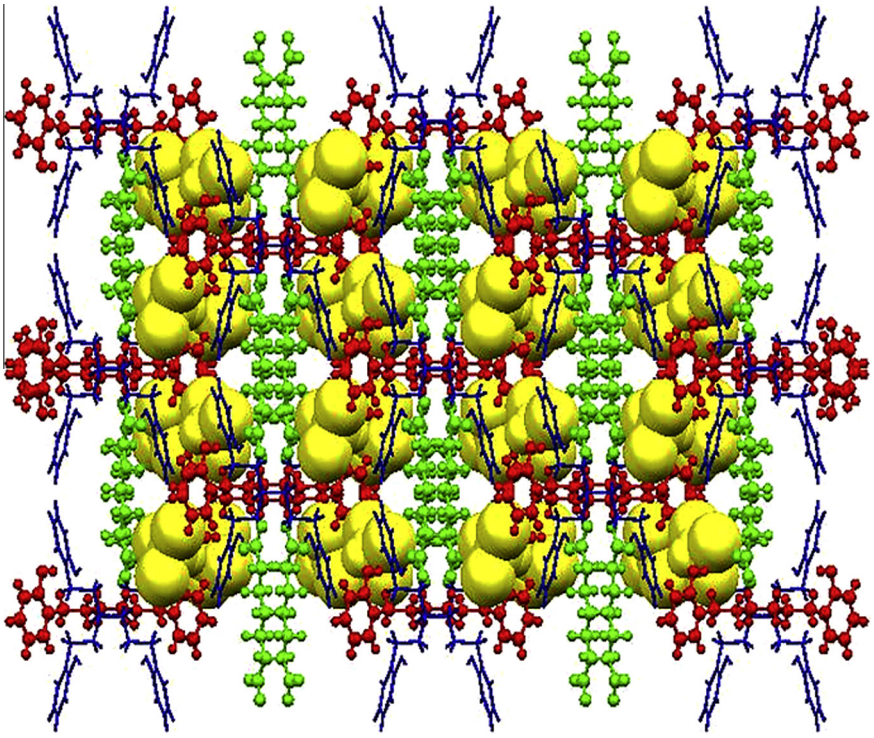

Fig. 4. Three dimensional mat like perspective view in **2**. Color code: protonated bases, red and blue; pimelate ion, green; $CHCl_3$, yellow. (For interpretation of the references to colour in this figure legend, the reader is referred to the web version of this article.)

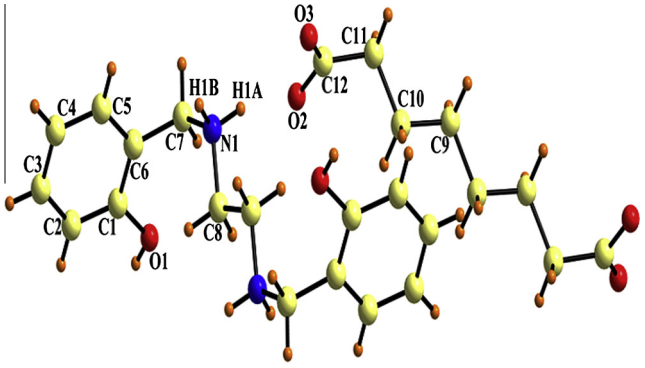

Fig. 5. Molecular structure of salt **3**. Color code: C, yellow; H, orange; O, red; N, blue. (For interpretation of the references to colour in this figure legend, the reader is referred to the web version of this article.)

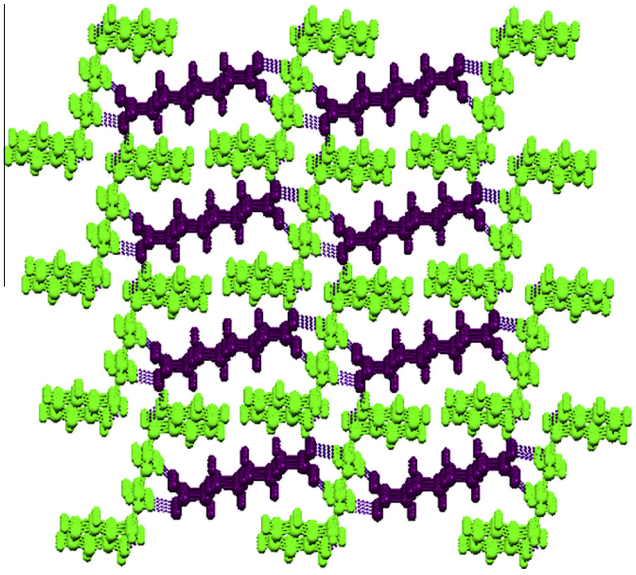

Fig. 6. Ladder like packing view with three different types of cavities in **3**. Color code: protonated base, green; suberate ions, purple. (For interpretation of the references to colour in this figure legend, the reader is referred to the web version of this article.)

two molecules of methanol solvent. In **4**, the acidic hydrogen of the carboxyl group on adipic acid was transferred to the nitrogen atom of base as shown in Fig. 7. According to Fig. 8(a), the phenolic oxygen (O1) and phenyl C—H of protonated base ($L_2H_2^{2+}$) are hydrogen bonded with the oxygen (O4) of methanol via O4—H4···O1, 2.888(9) Å; C4—H4A···O4, 3.162(9) Å and C5—H5···O4, 3.401(18) Å noncovalent interactions, respectively. The C—H of methanol is also noncovalently bonded with the oxygen atom (O1) of $L_2H_2^{2+}$ through C13—H13B···O1, 3.082(6) Å intermolecular interaction. All these interactions are resulted in the creation of square shaped pseudocavity of size 3.7 Å through $L_2H_2^{2+}$ and methanol molecules for the accommodation of guests (adipate ions). Adipate ions are resided in the cavity with the help of N—H···O [N1—H1A···O2, 1.810(8) Å; N1—H1A···O3, 2.816(5) Å; N1—H1B···O2, 2.087(2) Å] and C—H···O [C5—H5···O3, 3.469(9) Å; C7—H7A···O3, 2.933(6) Å; C9—H9A···O2, 2.532(9) Å; C9—H9B···O2, 3.116(8) Å] intermolecular interactions (Fig. 8(b)). Three dimensional host–guest supramolecular framework is formed along '*c*' axis with the help of these noncovalent interactions (Fig. 8c and d) [7].

The salt **5** with half molecule of protonated base ($L_2H_2^{2+}$) and half molecule of pimelate ion (PA^{2-}) in asymmetric unit crystallizes in monoclinic system with space group *C* 2/*c* as shown in Fig. 9. The two molecules of $L_2H_2^{2+}$ interact with each other via C8—H8B···π, 3.250(3) Å intermolecular interactions, and form a rectangular shaped cavity of size 1.4 Å for the insertion of pimalate ion (Fig. 10(a)). Guest ions are accommodated in the cavity with

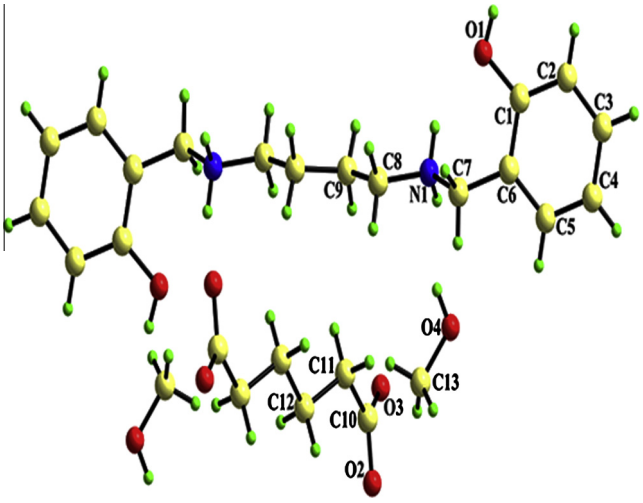

Fig. 7. Molecular structure of salt **4**. Color code: C, yellow; H, orange; O, red; N, blue. (For interpretation of the references to colour in this figure legend, the reader is referred to the web version of this article.)

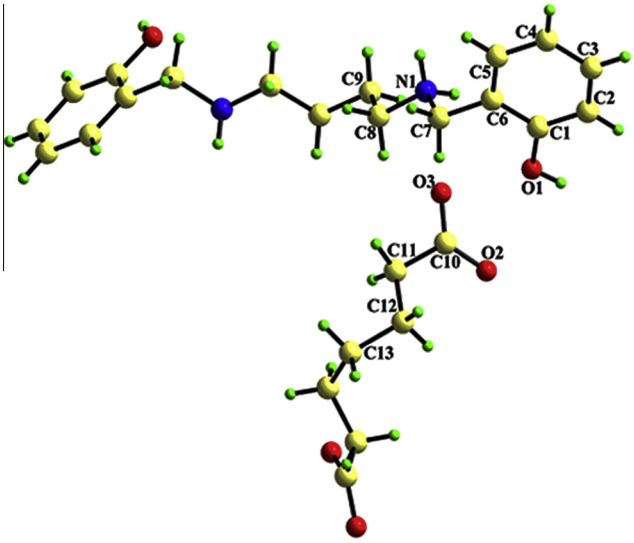

Fig. 9. Molecular structure of salt **5**. Color code: C, yellow; H, orange; O, red; N, blue. (For interpretation of the references to colour in this figure legend, the reader is referred to the web version of this article.)

the help of N—H···O [N1—H1A···O2, 1.949(4) Å; N1—H1B···O3, 1.898(2) Å] hydrogen bond interactions (Fig. 10(b)). Other noncovalent interaction O1—H1···O3, 1.815(6) Å is also present between cation and anion (Fig. S4). All these interactions provide the mat like host–guest supramolecular organic framework with and without guests along the '*c*' axis (Fig. 10c and d). The crystallographic packing view of this salt is similar to salt **4**.

Salt **6** crystallizes in monoclinic system with space group *C* 2/*c*, which contains half molecule of protonated base ($L_2H_2^{2+}$) and half molecule of suberate ion (SUA^{2-}) as shown in Fig. 11. According to Fig. 12(a), six molecules of $L_2H_2^{2+}$ are hydrogen bonded to each other through O1—H1···O1, 2.855(3) Å and C8—H8A···π, 3.541(10) Å noncovalent interactions, and form a spider shaped cavity of size 3.3 Å for the insertion of suberate ions as a guest. Two molecules of SUA^{2-} are accommodated in the cavity via N—H···O [N1—H1A···O3, 2.748(4) Å; N1—H1B···O2, 1.872(2) Å; N1—H1B···O3, 2.643(7) Å], O—H···O [O1—H1···O2, 1.860(3) Å] and C—H···O [C2—H2···O2, 2.765(6) Å; C9—H9A···O2, 2.923(10) Å; C11—H11A···O1, 2.647(8) Å] intermolecular interactions

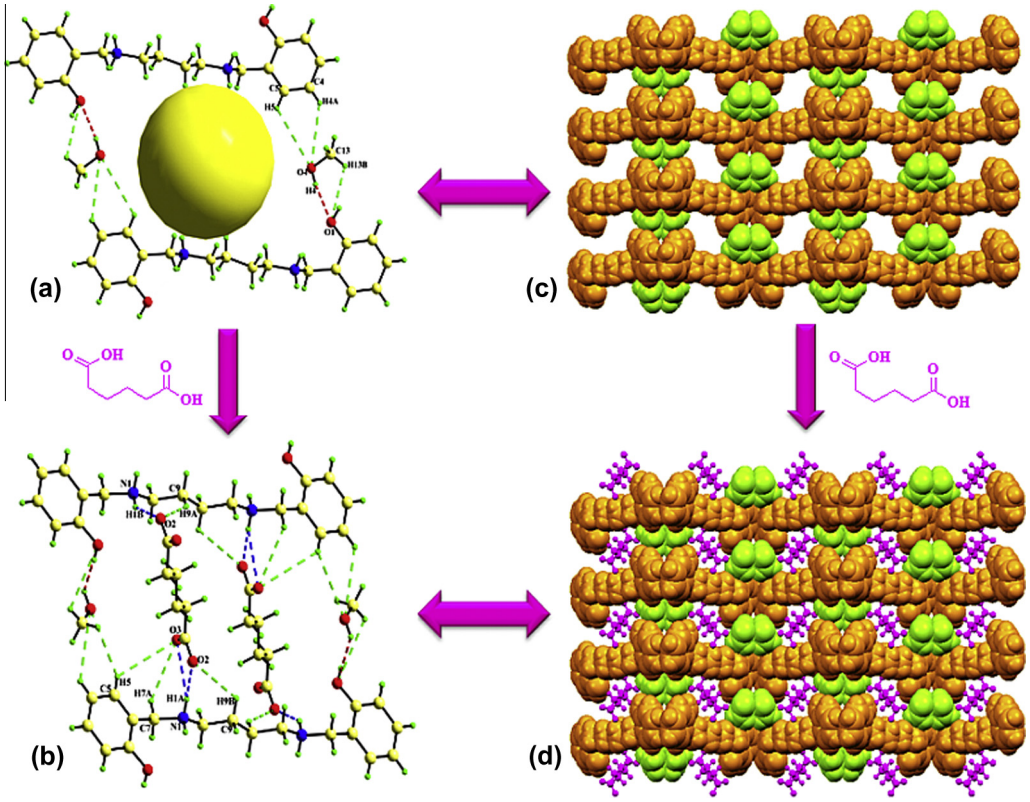

Fig. 8. (a) Square shaped cavity, (b) adipate ions in a cavity, (c) three dimensional host framework, and (d) three dimensional host–guest perspective view in **4**. Color code: protonated base, orange; adipate ion, pink; CH_3OH, green. (For interpretation of the references to colour in this figure legend, the reader is referred to the web version of this article.)

Please cite this article in press as: N. Goel, N. Kumar, J. Mol. Struct. (2014), http://dx.doi.org/10.1016/j.molstruc.2014.04.064

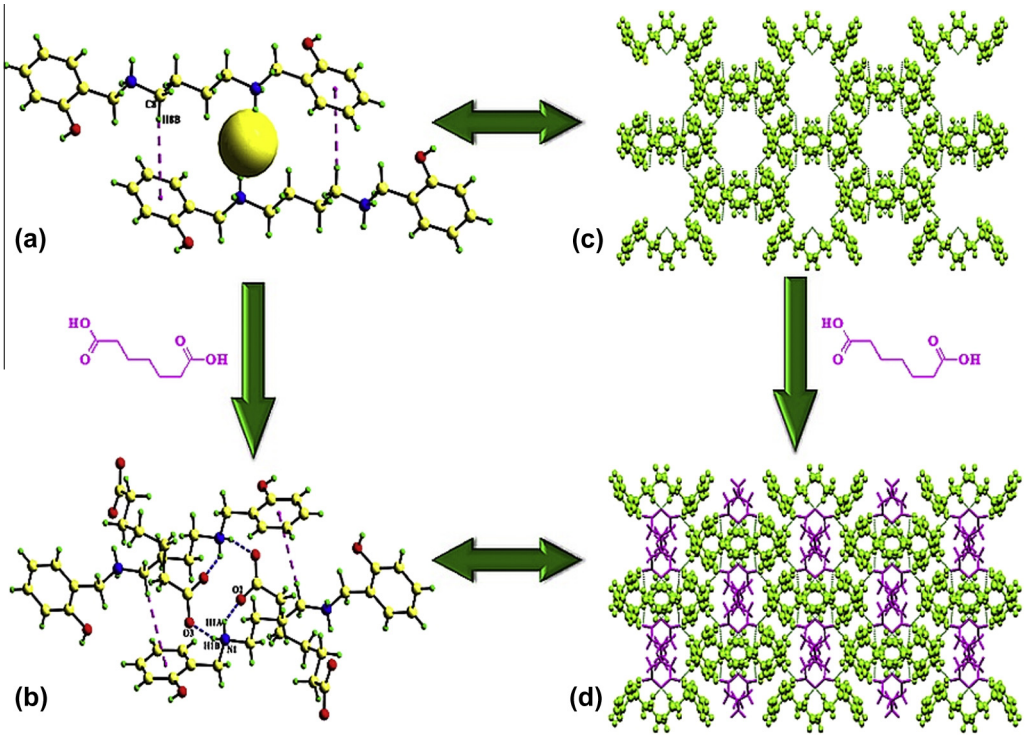

Fig. 10. (a) Rectangular shaped cavity, (b) pimalate ions in a cavity, (c) three dimensional host framework, and (d) three dimensional host–guest supramolecular architecture in **5**. Color code: protonated base, green; pimalate ion, pink. (For interpretation of the references to colour in this figure legend, the reader is referred to the web version of this article.)

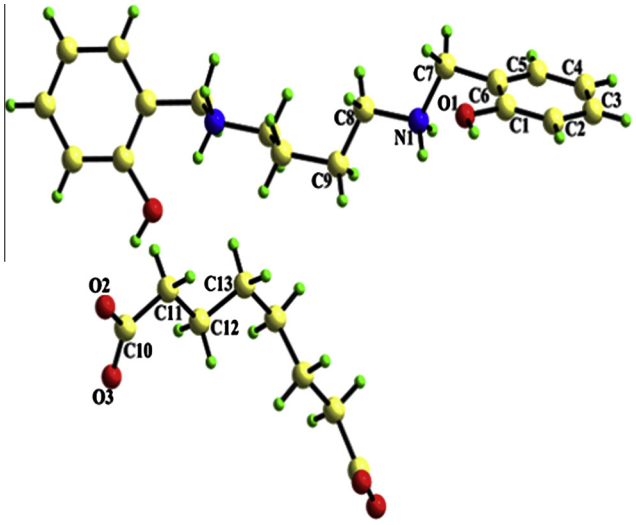

Fig. 11. Molecular structure of salt **6**. Color code: C, yellow; H, orange; O, red; N, blue. (For interpretation of the references to colour in this figure legend, the reader is referred to the web version of this article.)

(Fig. 12(b)). A similar hydrogen bonding motif is also present in salt **3**. Various hydrogen bonded interactions between protonated bases and suberate anions give the three dimensional supramolecular motif view along the '*c*' axis (Fig. 12c and d).

DFT and statistical analysis

The optimized geometry of salts **1–6** showed the positive harmonic vibrational frequencies, which suggested that the optimized structures were the global minimum on the potential energy surface. The single point energy calculations were performed for recording the zero point corrected total energies of various species. The optimized structures of salts **1–6** at B3LYP/6-311G^{++}(d,p) basis set are shown in Fig. 13. In addition to the characterization of these salts, the gas phase geometries, harmonic vibrational frequencies, and binding energies of these salts were also computed. The comparisons between experimental and simulated structural parameters such as bond lengths and bond angles are listed in Tables S3 and S4.

The hydrogen bond interaction energies were determined according to the following equation [8,9]

$$\Delta E = E_{salt} - (E_{acid} + E_{base})$$

where E_{salt}, E_{acid} and E_{base} are the zero point corrected total energies of salt, acid and base, calculated at B3LYP/6-311G^{++}(d,p) level of theory. We have removed the solvent and neutral molecules to check the relative stability. The trend observed for the hydrogen bond interaction energy is given in Table 3. DFT calculation shows that the hydrogen bond interaction energy decreases due to increase the carbon chain of both acids and bases i.e., CH_2 group is increased stepwise in each acid and base. This is because of *+I* effect, which makes the bond weak due to lengthening of the bond. Hence, the force constant becomes lower, and the energy decreases. Along with this, the negligible difference in the energy of the optimized structures and crystal structures of salts **1–6**, suggests that the orientation and interaction remain almost same in both the gas and solid phases (Table S5). From the statistical analysis, it is found that the value of correlation coefficient (*R*) for bond lengths are 0.966, 0.985, 0.944, 0.978, 0.946 and 0.964, while its values for bond angles are 0.989, 0.976, 0.959, 0.952, 0.974 and 0.981, respectively, in salts **1–6**. From this, it is clear that the theoretical (DFT) values are statistically closed to actual experimental (XRD) values. The plots for curve fitting analysis are given in Figs. S5-S8.

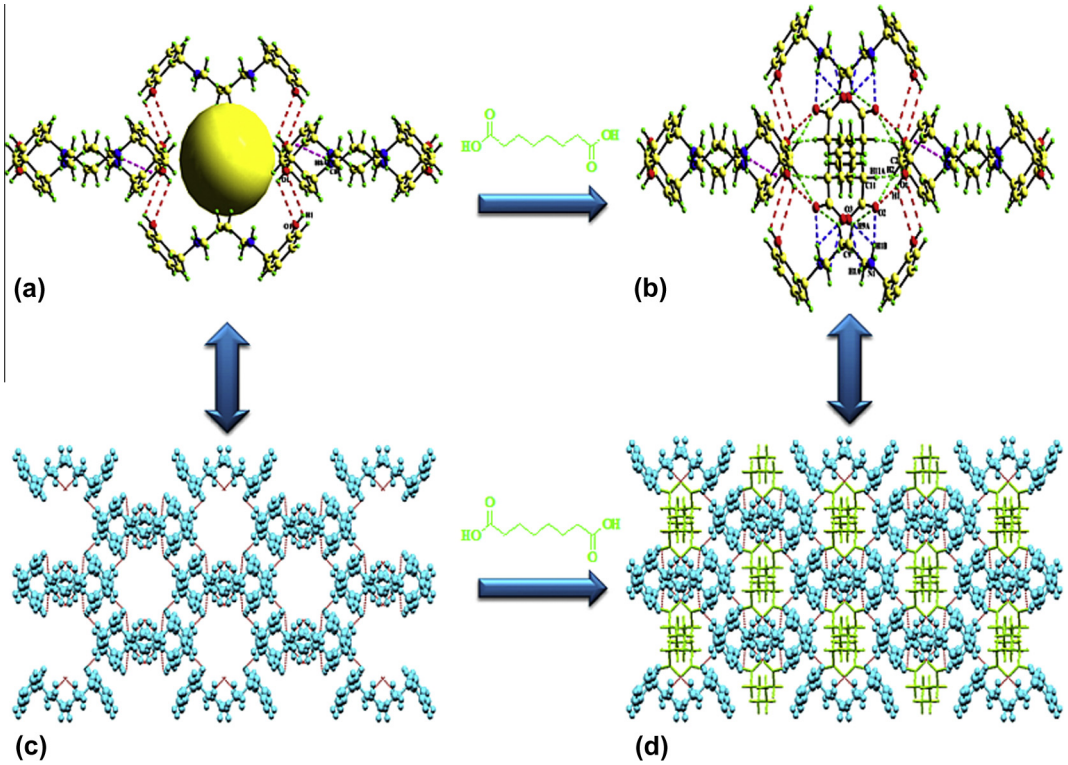

Fig. 12. (a) Spider shaped cavity, (b) suberate ions in a cavity, (c) three dimensional host framework, and (d) three dimensional host–guest view in **6**. Color code: protonated base, cyan; suberate ion, green. (For interpretation of the references to colour in this figure legend, the reader is referred to the web version of this article.)

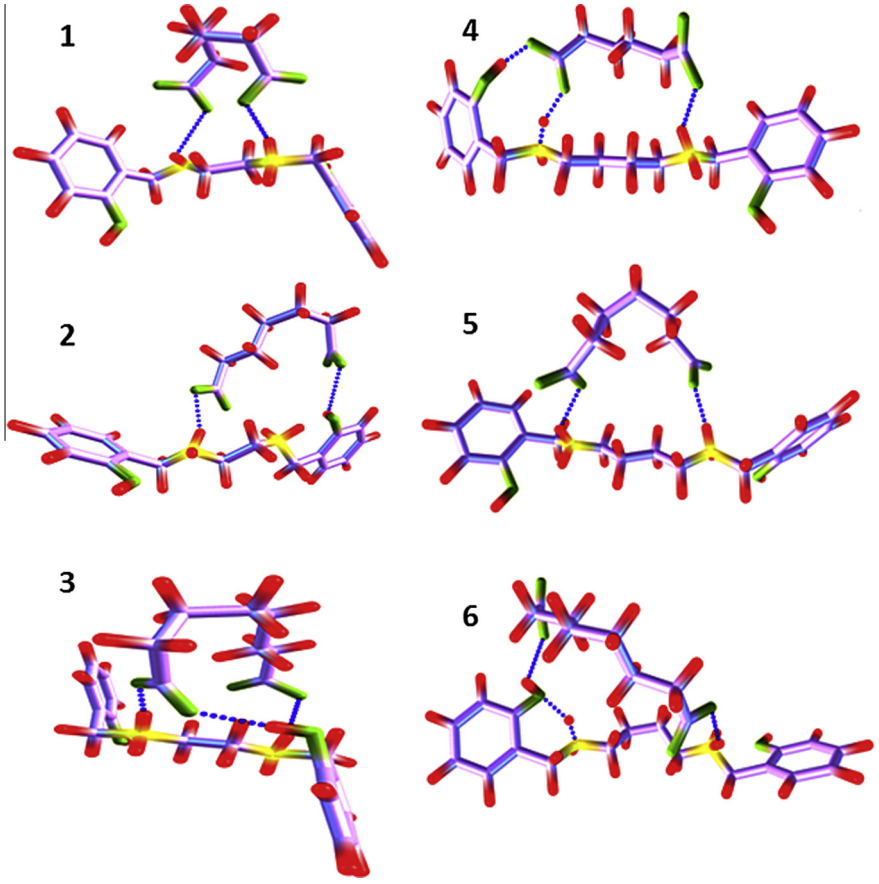

Fig. 13. Optimized geometry of salts **1–6**. Color code: C, pink; H, red; O, green; N, yellow. (For interpretation of the references to colour in this figure legend, the reader is referred to the web version of this article.)

Please cite this article in press as: N. Goel, N. Kumar, J. Mol. Struct. (2014), http://dx.doi.org/10.1016/j.molstruc.2014.04.064

Table 3
Hydrogen bond interaction energy of salts **1–6**.

S. no.	Salts	Hydrogen bond interaction energy (kcal/mol)
1	Salt **1**	30.48
2	Salt **2**	28.17
3	Salt **3**	25.75
4	Salt **4**	29.76
5	Salt **5**	26.82
6	Salt **6**	24.49

Table 4
TG–DTG data of salts **1–6** under a nitrogen atmosphere.

S. no.	Salts	TG			DTG
		T_i/°C	T_f/°C	α	Peak temp./°C
1	Salt **1**	157	214	24.3	194 °C
		329	423	72.9	377 °C
2	Salt **2**	151	174	20.9	121 °C
		215	369	77.4	253 °C
3	Salt **3**	198	347	98.7	324 °C
4	Salt **4**	134	207	12.1	160 °C
		355	437	86.6	379 °C
5	Salt **5**	294	429	98.4	367 °C
6	Salt **6**	213	352	98.6	341 °C

Thermal analysis

The thermal stability of salts **1–6** is demonstrated by TG–DTG. The thermoanalytical data are listed in Table 4, and the TGA–DTG curves are shown in Figs. S9 and S10. The thermograms clearly indicate that these salts are stable up to 100 °C but at higher temperatures, curves show irregular pattern. The thermal decomposition of salt **1** occurs in two steps. The first weight loss (24.3%) in the temperature range of 157 and 214 °C (DTG peak at 194 °C) corresponds to the release of neutral adipic acid. The second weight loss (72.9%) is observed in between 329 and 423 °C (DTG peak at 377 °C). It may be due to the release of protonated base and adipate ion. Salt **2** also undergoes two stages decomposition. The first stage (20.9% mass loss) corresponds to DTG peak at 121 °C. In this step chloroform (151–174 °C) leaves out. In the second stage (215–369 °C), both cation and anion are released (77.4% mass loss), which shows DTG peak at 253 °C. The thermal decomposition of salt **3** at temperature range 198–347 °C predicts the weight loss of 98.7% with the DTG peak at 324 °C due to the release of both protonated base and suberate ion. In salt **4**, first weight loss of 12.1% in between 134 and 207 °C (DTG peak at 160 °C) corresponds to the release of two methanol molecules. The second weight loss (86.6%) is observed in between 355 and 437 °C (DTG peak at 379 °C), and it may be due to the release of protonated base and adipate ion. Salt **5** undergoes one step decomposition with the loss of 98.4% in total mass, corresponds to DTG peak at 367 °C. In this step both cation and anion (294–429 °C) leaves out. The thermal decomposition of salt **6** (213–352 °C) shows the weight loss of 98.6% with the DTG peak at 341 °C due to the release of both protonated base and suberate ion.

Conclusions

In the present work, we have reported first time the structural characterization and computational studies of newly synthesized supramolecular frameworks having dicarboxylic acids, *N*,*N*′-bis(salicyl)ethylenediamine and *N*,*N*′-bis(salicyl)butylenediamine. The FT-IR and NMR spectroscopic results of salts **1–6** are in agreement with the result of X-ray crystallography i.e., existence of hydrogen bonding between donor and acceptor. From the statistical analysis, it is found that the theoretically calculated structural parameters are in line with the crystallographic data for salts **1–6**. The structural analysis reveals that the *N*,*N*′-bis(salicyl)ethylenediamine and *N*,*N*′-bis(salicyl)butylenediamine are excellent building blocks, which are responsible for the creation of entirely different three dimensional packing views. The diversity in supramolecular structures may be due to the difference in the carbon chain of carboxylic acids, bases, type of interactions and the orientation of the molecules in three dimensional spaces. From the three dimensional packing diagrams, it is cleared that the cavities with different shapes and size are created as the carbon chain increases in bases i.e., in salts **1–3**, there is no cavity but salts **4–6** have square to rectangular to spider shaped cavities. So the synthesis of these salts with pre-determined connectivity and topology will offer a path towards the design of materials with pre-determined bulk properties. Theoretical studies suggest that structures are same in both the gas and solid phases, and hydrogen bond interaction energy largely depends on the number of carbon chain i.e., hydrogen bond interaction energy decreases on increasing the chain length. Thermal study shows that all synthesized salts are stable at room temperature, and decompose at high temperature.

Acknowledgments

Authors gratefully acknowledge CSIR, New Delhi, India, for financial assistance in form of PDF to NG, SRF to NK and IITR for instrumental facilities.

Appendix A. Supplementary material

CCDC numbers 956403-956405 and 969961-969963 contain the supplementary crystallographic data (CIF) for this article. These data can be obtained free of charge from the Director, CCDC, 12 Union Road, Cambridge CB2 1EZ, UK (Fax: +44 1223 336 033; E-mail: deposit@ccdc.cam.ac.uk or http://www.ccdc.cam.ac.uk). Additional figures (Figs. S1–S10) and DFT calculations (Tables S1–S5) are available in PDF formats. Supplementary data associated with this article can be found, in the online version, at http://dx.doi.org/10.1016/j.molstruc.2014.04.064.

References

[1] P.A. Gale, Chem. Soc. Rev. 36 (2007) 141–142.
[2] A. Katsuhiko, K. Toyoki, Supramol. Chem.: Fundam. Appl. 173 (2006) 1–208.
[3] F. Vogtle, F. Alfter, Supramolecular Chemistry: An Introduction, Wiley, Chichester, New York, 1991.
[4] J.W. Steed, J.L. Atwood, Supramolecular Chemistry, Wiley, Chichester, New York, 2009.
[5] J.M. Lehn, Supramolecular Chemistry: Concepts and Perspectives, VCH, Weinheim, Germany, 1995.
[6] J.M. Lehn, Proc. Natl. Acad. Sci. 99 (2002) 4763–4768.
[7] U.P. Singh, N. Goel, G. Singh, P. Srivastava, Supramol. Chem. 24 (2012) 285–297.
[8] N. Goel, U.P. Singh, G. Singh, P. Srivastava, J. Mol. Struct. 1036 (2013) 427–438.
[9] N. Goel, U.P. Singh, J. Phys. Chem. A 117 (2013) 10428–10437.
[10] G.R. Desiraju, The Crystal as a Supramolecular Entity, Wiley, Chichester, New York, 1995.
[11] G.R. Desiraju, Crystal Engineering: The Design of Organic Solids, Elsevier, Amsterdam, 1989.
[12] T. Steiner, Angew. Chem. Int. Ed. 41 (2002) 49–76.
[13] T.L. Nguyen, F.W. Fowler, J.W. Lauher, J. Am. Chem. Soc. 123 (2001) 11057–11064.
[14] C.B. Aakeroy, A.M. Beatty, B.A. Helfrich, J. Am. Chem. Soc. 124 (2002) 14425–14432.
[15] G.A. Jeffery, W. Saenger, Hydrogen Bonding in Biological Structures, Spriger-Verlag, Berlin, 1991.
[16] G.A. Jeffery, An Introduction to Hydrogen Bondings, Oxford University Press, Oxford, 1997.
[17] L.J. Barbour, J.L. Atwood, Chem. Commun. 19 (2001) 2020–2021.
[18] M.W. Hosseini, Chem. Commun. (2005) 5825–5829.
[19] N.R. Goud, B.N. Jagadeesh, A. Nangia, Cryst. Growth Des. 11 (2011) 1930–1939.
[20] M.C. Etter, Acc. Chem. Res. 23 (1990) 120–126.

[21] S.S. Kuduva, D.C. Craig, A. Nangia, G.R. Desiraju, J. Am. Chem. Soc. 121 (1999) 1936–1944.
[22] T. Steiner, Acta Crystallogr. B 57 (2001) 103–106.
[23] T. Lee, P.Y. Wang, Cryst. Growth Des. 10 (2010) 1419–1434.
[24] L. Orola, M.V. Veidis, I. Mutikainen, I. Sarcevica, Cryst. Growth Des. 11 (2011) 4009–4016.
[25] A. Alhalaweh, S. George, D. Bostrom, S.P. Velaga, Cryst. Growth Des. 10 (2010) 4847–4855.
[26] T. Friscic, A.V. Trask, W.D.S. Motherwell, W. Jones, Cryst. Growth Des. 8 (2008) 1605–1609.
[27] A. Delori, E. Suresh, V.R. Pedireddi, Chem. Eur. J 14 (2008) 6967–6977.
[28] D.K. Bucar, R.F. Henry, X. Lou, T.B. Borchardt, G.G. Zhang, Chem. Commun. 5 (2007) 525–527.
[29] K.J. Paluch, L. Tajber, C.J. Elcoate, O.I. Corrigan, S.E. Lawrence, A.M. Healy, J. Pharm. Sci. 100 (2011) 3268–3283.
[30] D. Braga, G. Palladino, M. Polito, K. Rubini, F. Grepioni, M.R. Chierotti, R. Gobetto, Chem. Eur. J. 14 (2008) 10149–10159.
[31] M.L. Cheney, D.R. Weyna, N. Shan, M. Hanna, L. Wojtas, M.J. Zaworotko, Cryst. Growth Des. 10 (2010) 4401–4413.
[32] M.M. Sow, O. Diouf, I.E. Thiam, M. Gaye, P. Retailleau, Acta Crystallogr. E68 (2012) m121–m122.
[33] M.R.A. Pillai, C.L. Barnes, E.O. Schlempe, Polyhedron 13 (1993) 701–708.
[34] G.M. Sheldrick, SADABS, University of Göttingen, Göttingen, Germany, 1996.
[35] G.M. Sheldrick, Acta Crystallogr. A 46 (1990) 467–473.
[36] G.M. Sheldrick, SHELXTL-NT, Version 6.12, Reference Manual, University of Göttingen, Göttingen, Germany, 2000.
[37] K. Brandenburg, DIAMOND, Version 2.1c, Visual Crystal Structure Information System, Crystal Impact GbR, Bonn, Germany, 2000.
[38] MERCURY, Cambridge Crystallographic Data Centre, 12 Union Road, Cambridge CB2 1EZ, UK. <http://www.ccdc.cam.ac.uk/>.
[39] A.D. Becke, J. Chem. Phys. 98 (1993) 5648–5652.
[40] M.J. Frisch et al., Gaussian 09, Revision A.1, Wallingford, CT, 2009.
[41] C. Peng, P.Y. Ayala, H.B. Schlegel, M.J. Frisch, J. Comput. Chem. 17 (1996) 49–56.
[42] C. Ikeda, N. Nagahara, E. Motegi, N. Yoshioka, H. Inoue, Chem. Commun. 43 (1999) 1759–1760.
[43] R.M. Silverstein, G.C. Bassler, T.C. Morrill, Spectrometric Identification of Organic Compounds, fifth ed., John Wiley, New York, 1991.
[44] K. Nakanishi, P.H. Solomon, Infrared Absorption Spectroscopy, second ed., Emerson-Adams Press Inc., 1977.
[45] J.C. MacDonald, P.C. Dorrestein, M.M. Pilley, Cryst. Growth Des. 1 (2001) 29–38.
[46] B. Ji, W. Wang, D. Deng, Y. Zhang, Cryst. Growth Des. 11 (2011) 3622–3628.
[47] A. Mukherjee, G.R. Desiraju, Cryst. Growth Des. 11 (2011) 3735–3739.
[48] P. Sanphui, S. Tothadi, S. Ganguly, G.R. Desiraju, Mol. Pharm. 10 (2013) 4687–4697.

Please cite this article in press as: N. Goel, N. Kumar, J. Mol. Struct. (2014), http://dx.doi.org/10.1016/j.molstruc.2014.04.064